Active Antenna for Contact Sensing

Makoto Kaneko, *Member, IEEE,* Naoki Kanayama, and Toshio Tsuji, *Associate Member, IEEE*

Abstract— This paper proposes a new active sensor system (active antenna) that can detect not only the contact location between an insensitive flexible beam and an environment but also the information of the environment's surface where the beam makes contact. The active antenna is simply composed of a flexible beam, actuators to move the beam, position sensors to measure the rotational angle of the beam, and a moment sensor. We first show that the contact distance under no lateral slip is proportional to the rotational compliance that the beam can sense at the rotational center. The lateral slip, which possibly occurs according to the pushing direction and the environment's geometry, overestimates the rotational compliance, and as a result, brings a large sensing error for the localizing contact point. The goal of this paper is to find the contact location under such conditions. We explore how to detect a lateral slip and how to determine the new pushing direction to avoid it. We show an algorithm that can search for the pushing direction which can avoid any lateral slip. The convergence of this algorithm is shown and a practical utilization of this algorithm is also discussed with a trade-off between the number of trials and the sensing accuracy.

Index Terms— Active antenna, contact point sensing, tactile sensing.

I. INTRODUCTION

PLURAL eyes which are the vision system for insects, may work effectively in either detecting the rough shape of object or confirming the existence of object. However, it is well known that they can neither recognize the precise shape of an object nor measure the distance up to the object. On the other hand, insects have two advanced antennae that can compensate for the limitation of the sensing capability by their vision system. Furthermore, insects seem to use their antennae skillfully so that they may avoid colliding with objects particularly close to them. An interesting observation is that insects are always moving their flexible antennae actively as shown in Fig. 1, while crawling, running, and even staying still. The antenna can be characterized by its *flexibility* and *active motions*. Active motions might be useful for extending the sensing volume in three-dimensional (3-D) space, and the flexibility of the antenna would contribute to reducing the impulsive force appeared when the antenna contacts an object unexpectedly. While insect's antenna possesses these inherent advantages, our main goal is to propose a new active sensing system, in which both *flexibility* and *active motions* essentially contribute to localizing contact point between the antenna and environment.
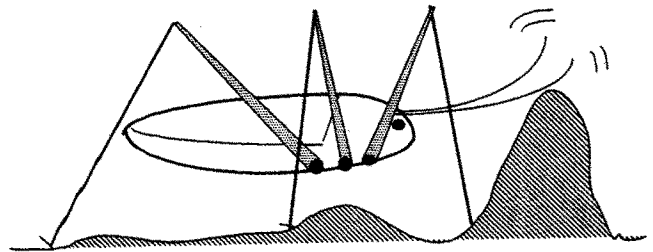
Fig. 1. Insect's antennae.

There have been a number of works discussing insect's antennae-like sensor or whisker type sensor. For example, a simple flexible beam sensor can take the form of a short length of spring piano wire or hypodermic tubing anchored at the end. When the free end touches an external object, the wire bends. This can be sensed by a piezoelectric element or by a simple switch [1]. A more elaborate sensor is described by Wang and Will [2]. Russell designed articulated whisker probes [3] which can measure the outline of objects. As far as we know, this is the first work that demonstrated the capability of providing detailed outline images of small objects by whisker type sensor, while it is assumed that the whisker tip is always in contact with objects. Long antennae-like whisker sensors were mounted on the SRI mobile robot, Shakey [4], and on Rodney Brook's six-legged robot insects [5]. Hirose *et al.* discussed the utilization of whisker sensors in legged robots [6]. The sensor system is composed of an electrode and a whisker whose end is fixed at the base. This sensor unit has been arranged in an array around each foot of the legged robot, Titan III, so that it can monitor the separation between each foot and the ground to allow deceleration of the foot before contact. This sensor is also conveniently used to confirm which part of the foot is in contact with the ground. Similarly shaped whiskers have been considered for legs of the Ohio State University active suspension vehicle [7]. Russell has developed a sensor array [8] by mounting whisker sensors on a mobile robot, and succeeded in reconstructing the shape of a convex object followed by the whisker. In his work, it is assumed that the whisker tip is always in the environment, and that when the whisker contacts the environment except for the tip, it is assigned to a failure mode. Wilson and Mahajan [9], Snyder and Wilson [10] have designed the whisker probe system composed of a piano wire with strain gauge sensors and the base sweep actuators made of two polyurethane tubes that bend when pressurized with air. Wilson and Chen [11] have reported experimental results that demonstrate the precision and accuracy of the whisker probe system in detecting and displaying solid boundaries enclosing areas up to 40 by 50 cm. These works also assume that the whisker tip always

makes contact with the object. The major difference between previous works [1]–[11] and ours is that the active antenna can localize a contact point between the insensitive antenna and the environment, while previous works do not.

Concerning the contact point localization, there have been several works. All of them can be categorized into either the passive sensing or the active one. As for passive sensing, Tsujimura and Yabuta have addressed an object shape detection system using a six-axis force/moment sensor and an insensitive flexible probe [12]. This approach is based on the original idea that a six-axis force/moment information makes it possible to estimate a contact location as well as a contact force, which was first pointed out by Salisbury [13] and later extended more general and mathematical forms by Brock and Chiu [14], Tsujimura and Yabuta [15], and Bicchi [16]. However, the utilization of six-axis force/moment sensor is generally expensive and requires a carefully prepared calibration matrix data so that we can compute the contact information with high accuracy. Also due to the direct use of force/moment sensor output, both the drift and noise are inherently involved in the output signal, and this deteriorate the sensing robustness. As for active sensing, Kaneko and Tanie [17], [18] have proposed an approach to detect contact point between a finger link and an object by using strategic link motions. A finger link having a compliant joint can change its posture while maintaining contact between the link and the object, when imparting an angular displacement to a proper joint. From two link postures before and after strategic link motions, we can compute the intersection between two links, which provides us with an approximate contact point. Kaneko, Maekawa, and Tanie [19], Maekawa et al. [20] have shown different approaches with assuming a finger tip tactile sensor.

An active antenna is composed of an insensitive flexible beam, actuators to move the beam, position sensors to measure the beam position, and a two (at most)-axis moment sensor to evaluate the contact force. To understand the sensing principle of the active antenna intuitively, let us consider a simple example. Suppose that we grasp a flexible beam like a fishing rod by one hand. When the beam makes contact with an object close to the grasping point, we feel a stiff resistance to pushing motion. On the other hand, when the contact happens close to the tip, we feel relatively large compliance. This means that the rotational compliance which we can feel at our hand is a function of contact position. Thus, the active antenna is a sensing system enabling us to detect the contact location through the measurement of the rotational compliance of an insensitive flexible antenna in contact with an environment. Since we can not measure the rotational compliance without imparting a proper active motion, active motions are quite essential for the proposed sensing system. The flexibility of the antenna is also quite essential, because the rotational compliance never changes according to the contact location without the distributed flexibility of the antenna. One big advantage of active antenna is that the contact point sensing is achieved through a surprisingly simple active motion and is not required any complicated motion planning. This is because the flexibility of the antenna successfully absorbs the contact force, even under a large positional error.
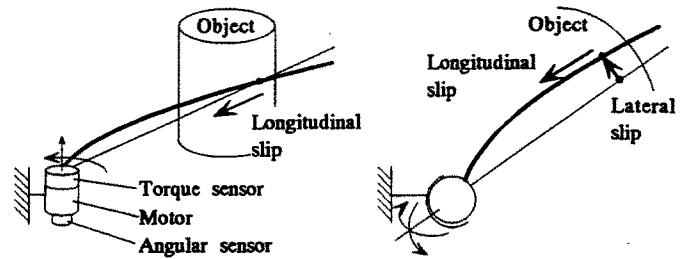

Fig. 2. Basic behaviors of a flexible beam during a pushing motion for an environment.

At the beginning of sensing, the antenna approaches an environment until it makes contact. Since this approach phase is exactly the same as the one discussed in other tactile based active sensing [17]–[19], we do not repeat this phase again in this paper. We suppose that at the initial state, the antenna is already in contact with the environment. Fig. 2 shows two examples of pushing motions, where (a) and (b) correspond to a two-dimensional (2-D) and a 3-D active antenna [21], [22], respectively, where the antenna's motion is restricted in a plane for a 2-D model while it can sweep in 3-D space for a 3-D one. While imparting a pushing motion for a 2-D active antenna, a longitudinal slip inevitably appears to satisfy the geometrical relationship between the antenna shapes before and after a bending deformation. While applying a pushing motion for a 3-D one, however, a lateral slip may occur in addition to a longitudinal slip. The lateral slip, which is the inherent characteristic for 3-D active antenna, strongly depends on the direction of pushing, the friction at the point of contact, and the normal surface of the environment where the antenna makes contact. Generally, such a lateral slip overestimates the rotational compliance of the antenna in contact with the environment and, as a result, deteriorates the sensing accuracy. On the contrary, the longitudinal slip brings a minor error only. Our goal in this paper is to find the contact location between the antenna and the environment under these conditions. Therefore, one of the key issues in this paper is how to detect the lateral slip by using the implemented sensors. Once any lateral slip is detected, one active motion is no longer sufficient and more than two active motions are necessary for localizing the contact point. This is because the rotational compliance is no longer a function of the contact point alone, and varies according to how much and to which direction the lateral slip occurs. The basic idea taken in the paper is to eventually find the direction that avoids any lateral slip during the active motions. Thus, another important issue of this paper is to explore the sensing algorithm that can finally reach the pushing direction avoiding any lateral slip. Once we find such a direction, the problem results in that of a 2-D model, since the antenna's motion is restricted in a plane. As a result, the contact point can be obtained through the measurement of rotational compliance during the last pushing motion where no lateral slip is detected. Therefore, we can block out a lateral slip only if a pushing motion is imparted to the normal direction of the environment. Thus, if we can find the direction which does not have any lateral slip, we can obtain both the contact location and the surface including the normal direction simultaneously.

This paper is organized as follows. After defining active sensing, we explain the basic working principle of active antenna using a 2-D planar model in Section II. In Section III, we address a general 3-D active antenna with its mechanical structure and its basic sensing algorithm considering a lateral slip. In Section IV, we deal with the effect of environment curvature on the sensing accuracy before concluding the paper. In Section V, we discuss how to cope with a compliant object.

II. NECESSITY OF ACTIVE MOTIONS AND BEAM FLEXIBILITY

In this section, we explain why both active motions and beam flexibility are essential for localizing a contact point. Our basic group A Assumptions are listed as follows.

A-1: The object is rigid.

A-2: The deformation of the beam is small enough to ensure that we can apply classical beam theory.

A-3: The environment (called also as object) to be sensed is stationary during active motions.

A-4: The elongation of the beam due to a unit axial force is negligibly small compared with the deflection due to a unit bending force.

A-5: Before imparting an active motion, the beam is already in contact with an environment with zero contact force.

A-6: The beam is connected to the actuator shaft at the center of rotation.

A-7: The beam's motion is limited to a plane.

A-8: The pushing motion is applied to the normal direction of the environment.

A-9: The beam makes contact with an edged environment.

Assumption A-1 is quite essential, since the proposed scheme cannot decompose the sensed compliance into the one coming from the beam itself and the other from the environment. Assumption A-2 can be conveniently utilized when extracting a simple result from a set of nonlinear equations. Since a piano-wire like beam can deform easily for a bending force, Assumption A-3 can exist for most of practical cases. Assumption A-4 implies that the antenna is extremely stiff in its axial direction, while it is very compliant in nonaxial direction. Assumption A-6 is necessary for avoiding the complicated formulation. For practical application, however, the sensing system needs a proper adaptor for connecting an actuator with a beam. Such an adaptor has a large stiffness compared with the beam and, as a result, brings a complicated relationship between the contact length and the rotational compliance. In order to understand the true nature of an active antenna, we assume a 2-D model with Assumption A-7. But this assumption is removed in Section III when discussing the 3-D model. Assumption A-8 is for avoiding any lateral slip at the point of contact. With Assumption A-9, we can neglect the effect of the shift of contact point on the environment, while it always changes along the beam. We consider the effect of the environment's curvature later part, in Section IV. We hold Assumptions A-1, A-2, A-3, A-4, and A-5 through this paper, while four others are either relaxed somehow or removed later.

Let us now consider a beam element in contact with an object as shown in Fig. 3, where (a) and (b) are rigid and
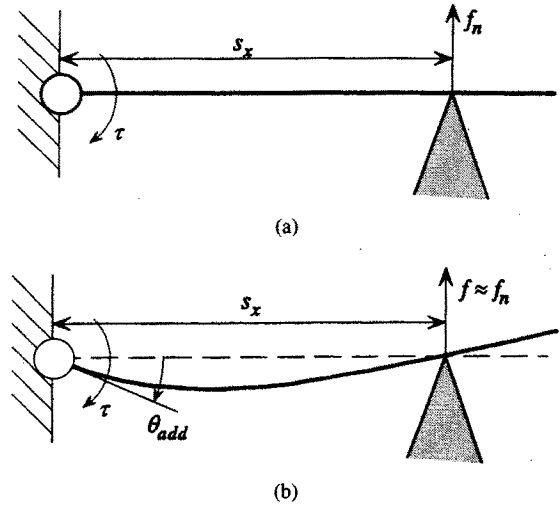

Fig. 3. Difference in behavior of rigid and flexible beams under increasing the joint torque.

flexible beams, respectively. When a beam contacts an object, a contact force will appear between the beam and the object. As a result, the actuator receives a reaction torque generated by the contact force. This torque τ is given by

$$\tau = f_n s_x \qquad (1)$$

where f_n and s_x are the force component normal to the beam and the distance from the beam fixed end to the contact point. Equation (1) includes two unknown parameters, i.e., f_n and s_x. Even when we can detect τ, we can not decompose it into f_n and s_x, if the beam is rigid. Thus, we can not determine the contact distance s_x under a rigid beam. Let us now consider a flexible beam as shown in Fig. 3(b). For such a flexible beam, we can impart an additional angular displacement θ_{add} to the beam even after it contacts an environment. Under a constant angular displacement θ_{add}, we can expect a marked increase in contact force especially when the contact point is close to the face of the beam, while it will be small when it is close of the beam's tip. For an arbitrary contact point, we can expect a larger contact force for a larger pushing angle θ_{add}. This means that the contact force is a function of the contact distance s_x and the pushing angle θ_{add}, which yields

$$f_n = F_1(s_x, \theta_{add}) \qquad (2)$$

where F_1 is determined by force-deformation relationship of the beam. From (1) and (2), we can eliminate f_n and finally obtain

$$s_x = F_2(\tau, \theta_{add}). \qquad (3)$$

If we assume a torque sensor and an angular sensor at the base, the right hand term becomes known and thus, we can obtain the distance up to the contact point along the beam. For example, let us assume a flexible beam whose cross section is uniform along the beam. For such a beam, (2) can be rewritten by

$$f_n = \frac{3EI\theta_{add}}{s_x^2} \qquad (4)$$

where E and I are the elasticity and second order moment of cross section of the beam, respectively. Therefore, we can get

$$s_x = 3EI \frac{\theta_{add}}{\tau}. \tag{5}$$

Equation (5) is quite simple but it tells us an important relationship. Namely, the distance s_x is in proportion to the angular displacement θ_{add} and in inverse proportion to the joint torque τ. To obtain a more compact form, we introduce the following relationship between τ and θ_{add}

$$\theta_{add} = C_\theta \tau \tag{6}$$

where C_θ is the so called rotational compliance. Substituting (6) into (5), we obtain

$$s_x = kC_\theta \tag{7}$$

where $k = 3EI$. Equation (7) implies that the distance s_x is simply in proportion to the rotational compliance of the beam in contact with the environment. In other words, the compliance changes linearly according to the contact length.

Note that neither (5) or (7) can be derived without both beam *flexibility* and an *active motion*. In other words, an active motion for a flexible beam enables us to decompose the torque τ into f_n and s_x, respectively.

Let us now briefly explain the effect of friction force on the measurement of the contact point. A contact force can be separated into normal and tangential components, while the above discussion focuses on the normal component alone. The tangential component brought by a frictional force is not uniquely determined but varies according to the contact condition where the beam makes contact. When a straight beam is used, we can neglect the effect of friction force, because a tangential force makes only a negligibly small moment around the torque sensor as far as the beam deformation is small enough (Assumption A-3). This is not the case for a curved beam, since both normal and tangential force components contribute to producing nonnegligible moments around the torque sensor. As a result, the rotational compliance is the function of the friction coefficient at the point of contact as well as the contact distance. Now, we summarize an important remark; *For straight antenna, it is always, possible to localize the contact point irrespective of the friction at the point of contact (Friction robustness for sensing). For curved antenna, the contact point sensing is influenced by friction at the point of contact.*

In the case of a straight antenna, a lateral load produces a well defined deflection proportion to the load. However, the antenna will be able to support a much larger axial load with little deflection because of extremely high stiffness in such a direction. At some poorly defined critical value of axial load the antenna will buckle and collapse. Furthermore, since such an axial load generates no torque around the torque sensor, this situation can not be monitored by the installed sensors. While there exists such a disadvantage for utilizing a straight antenna, we believe that it is important to take the advantage of the friction robustness in sensing by a straight antenna and, therefore, assume the straight antenna hereafter.
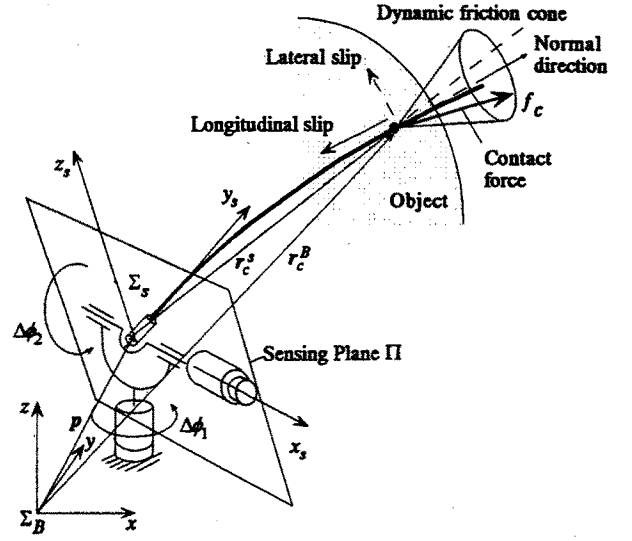

Fig. 4. Basic structure and its coordinate system of 3-D active antenna.

III. BASIC STRUCTURE AND WORKING PRINCIPLE OF 3-D ACTIVE ANTENNA

A. Basic Structure

Fig. 4 shows a schematic of the 3-D active antenna and its coordinate system, where Σ_B (or superscript "B") and Σ_s (or superscript "s") denote the base coordinate system and the sensor coordinate system, respectively. The 3-D active antenna is composed of an flexible beam, two actuators to move the beam in 3-D space, two position sensors to measure the angular displacements ϕ_1 and ϕ_2, and a two-axis moment sensor to detect moments around both x_s and z_s axes. The moment sensor is designed so that each sensing axis can intersect with the center of rotation (the origin of the sensor coordinate system). Now, let us define the sensing plane Π, as the plane spanned by two unit vectors whose directions coincide with x_s and z_s. The design orientation taken for the two-axis moment sensor enables us to evaluate the direction of the contact force projected on the plane Π from the outputs of the moment sensor. Fig. 5 shows a picture of the developed 3-D active antenna which is composed of two DC servo motors, and a piano wire with the length of 210 mm and diameter of 0.8 mm, and a two-axis moment sensor. The design orientation of the antenna geometry is given in Appendix.

B. Main Assumptions

Here, we remove the Assumptions A-7, A-8, and A-9, since they are inherent assumptions for a 2-D model. Instead, we set the following additional group B Assumptions.

B-1: The antenna has a uniform compliance in a plane perpendicular to the longitudinal axis.

B-2: The environment has an extremely small curvature along the axial direction of the beam.

A uniform beam having a circular cross section, such as a piano wire can satisfy Assumption B-1. For such a beam, the direction of reaction force is exactly colinear with that of the beam deflection, which can be conveniently utilized for
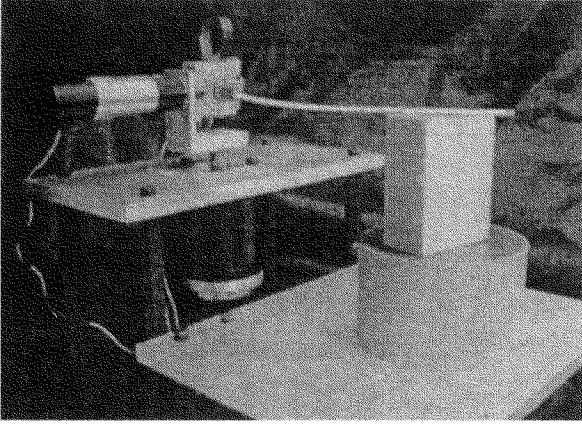
Fig. 5.   An overview of the developed 3-D active antenna.

Fig. 6.   Calibration result for an edged object without any lateral slip.

judging the occurrence of the lateral slip. With Assumption B-2, we neglect the effect of the environment's curvature on the sensing accuracy for simplifying the discussion. In Section IV, we will discuss the effect of environment's curvature on the sensing accuracy.

C. Basic Working Principle Without Lateral Slip

We have the following kinematic relationship between r_c^s and r_c^B:

$$\begin{bmatrix} r_c^B \\ 1 \end{bmatrix} = H \begin{bmatrix} r_c^s \\ 1 \end{bmatrix} \tag{8}$$

$$H = \begin{bmatrix} R & p \\ 0_{1\times3} & 1 \end{bmatrix} \tag{9}$$

where R and H are, respectively, the rotational matrix and the homogeneous transformation matrix representing both position and orientation of the sensor coordinate system with respect to the base coordinate system, and $0_{1\times3} = [0, 0, 0]$, and $p = [p_x, p_y, p_z]^t$, respectively. Since we can shift the origin of Σ_B to Σ_s without losing any generality, we set $p = [0, 0, 0]^t$ for simplicity. Then, (8) can be expressed as

$$r_c^B = Rr_c^s. \tag{10}$$

Let $r_c^s = [0, s_x, 0]^t$ be the contact point in Σ_s with the joint angles of ϕ_1 and ϕ_2 before imparting $\Delta\phi_1$ and $\Delta\phi_2$. Once s_x is detected, the contact point in Σ_B can be easily obtained by using the transformation matrix R between Σ_o and Σ_s. Thus, the main issue from now on is how to detect s_x.

Let Δm_x^s and Δm_z^s be the measured in elemental moment along the x_s and z_s directions, respectively. Then, the resultant moment in the sensing plane is simply

$$\|\Delta M\| = \sqrt{(\Delta m_x^s)^2 = (\Delta m_z^s)^2}. \tag{11}$$

With elementary beam theory and a beam of round cross section, we can obtain the following compact form between s_x and C_θ

$$s_x = 3EIC_\theta \tag{12}$$

where $C_\theta = \theta_{add}/\|\Delta M\|$, with $\theta_{add} = \|\Delta r_c^s\|/s_x = \sqrt{\Delta\phi_1^2 = \Delta\phi_2^2}$. Equation (12) is exactly the same as (7)

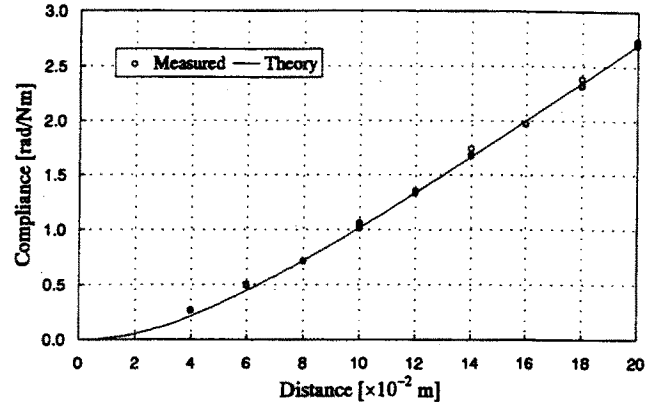obtained for the 2-D model. Thus, under no lateral slip, the working principle of the 3-D model reduced to that of 2-D model, as expected.

Fig. 6 shows an example of calibration results obtained under no lateral slip, where the real line denotes the theoretical result and the circles denote experimental data for five trials. It can be seen from Fig. 6 that the agreement between theoretical and experimental results are fairly good and the repeatability of experiments is also fine. It should be noted that there exists a small nonlinear effect between the contact distance and the rotational compliance, while the analysis under Assumption A-6 shows that the contact distance is purely proportional to the rotational compliance. This nonlinearity comes from the existence of the adaptor between the actuator shaft and the beam. The theoretical line in Fig. 6 is obtained by considering the geometry of the adaptor [21].

D. Basic Working Principle Under Lateral Slip

1) Lateral Slip and Its Effect on Contact Sensing: The antenna is extremely stiff in the longitudinal direction and is not elongated along the direction of an axial force (Assumption A-4), while it easily deforms for a bending moment. When the angular displacements, $\Delta\phi_1$ and $\Delta\phi_2$, are imparted to the antenna, it deforms while keeping contact as shown in Fig. 4. During this pushing motion, it continuously makes a longitudinal slip on the point of the contact to the environment. This allows us to consider only the case of the dynamic friction cone during the whole active motion.

Fig. 7 shows the relationship among the virtual displacement vector Δr_v^s, the effective displacement vector Δr_e^s and the dynamic friction cone after a pushing motion, where α is the angle of the dynamic friction cone. Fig. 8 shows several physical parameters projected on the sensing plane Π, where ν^+, ν^-, ψ, and φ denote the outer and the inner normal directions of the environment's surface, the direction of Δf_c^s, and the pushing direction with respect to Σ_s, respectively. Since we assume the uniform compliance by Assumption B-1, the contact force on Π always appears in the opposite direction against the effective displacement vector Δr_e^s. This means that the contact point moves in such a way that Δr_e^s and Δf_c^s are colinear. It should be noted that the force projected on the sensing plane can exist either on the boundary or within the
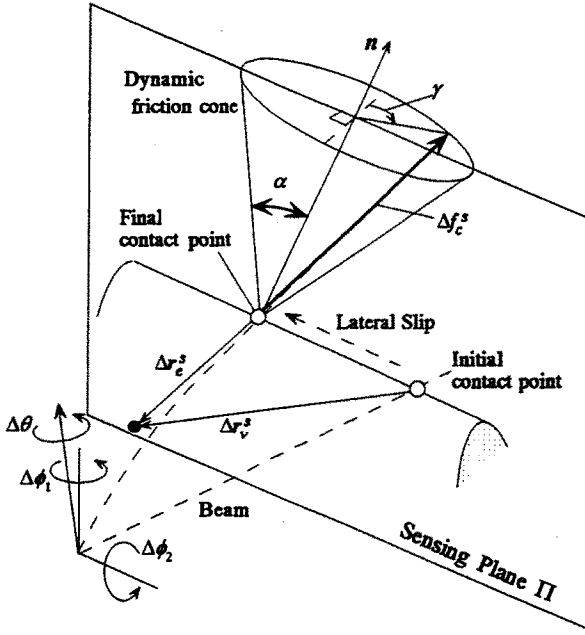
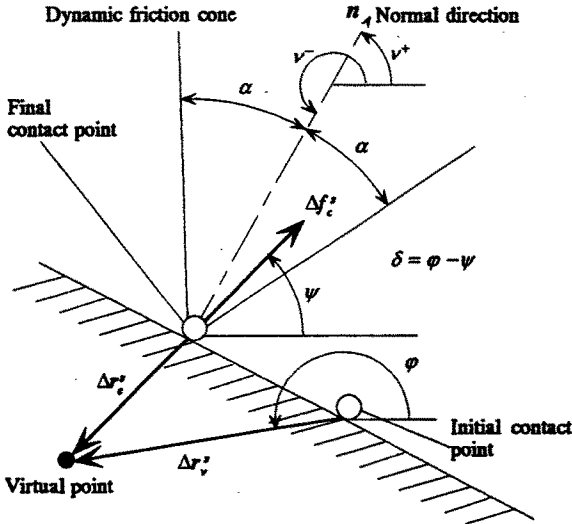Fig. 7. A general view of 3-D active antenna when a lateral slip occurs.

Fig. 8. Notations on the sensing plane Π.

Fig. 9. Three patterns of the contact states.

projected cone, while the contact force always exists on the boundary of the dynamic friction cone. Since $\|\Delta r_v^s\| > \|\Delta r_e^s\|$ under lateral slip, $\Delta f_c^s(\|\Delta r_v^s\|) > \Delta f_c^s(\|\Delta r_e^s\|)$, which means that the contact force under no lateral slip is always larger than that under lateral slip. Thus, the rotational compliance is generally overestimated under lateral slip. As a result, the sensing accuracy will deteriorate. This shows the difference between a 2-D and a 3-D active antenna.

2) Judgement of Contact States: Before conducting an analysis of the lateral slip, we make clear what physical parameters we can measure by utilizing the implemented sensors. There are two physical parameters obtained by the sensors, the direction of the contact force ψ and the pushing direction φ.

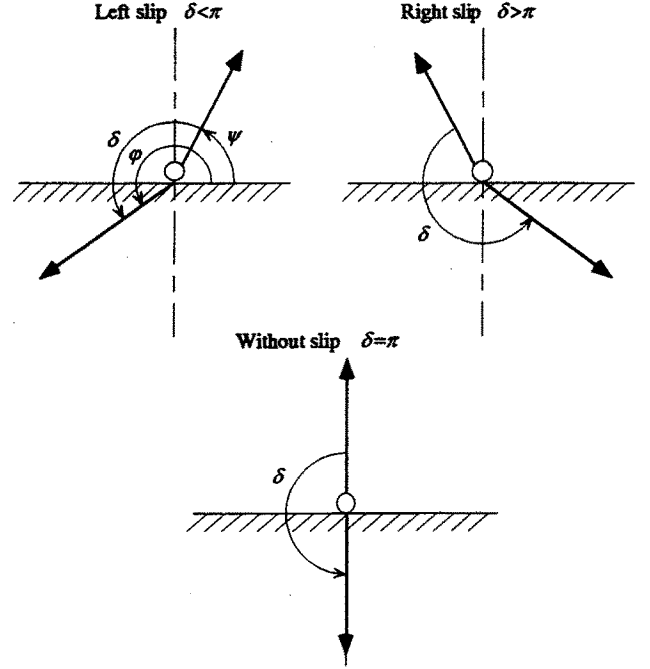*a) Direction of contact force projected on Π, ψ:* From the force-moment balance equation, the following relationship

exists:

$$\frac{\Delta m_x^s}{-\Delta m_z^s} = \frac{\Delta f_z^s}{\Delta f_x^s} \tag{13}$$

$$\psi = \tan^{-1}\left(\frac{\Delta f_z^s}{\Delta f_x^s}\right) = \tan^{-1}\left(\frac{\Delta m_x^s}{-\Delta m_z^s}\right). \tag{14}$$

Since both Δm_x^s and Δm_z^s can be measured by the moment sensor, we can obtain the direction of the contact force projected on the sensing plane Π.

b) How to detect lateral slip: Since each actuator has a position sensor, the pushing direction can also be measured. The pushing direction φ can be regarded as an input for this sensor system, and it provides the direction of contact force ψ as an output. There are three patterns for judging the contact states, as shown in Fig. 9. Let δ be the difference between ψ and φ. If δ is less than π, it means that the antenna slips in the left direction. If δ is greater than π, it means that the antenna slips in the right direction. If δ is equal to π, it means that there is no slip during the pushing motion. Based on this information, the next pushing direction is determined so that we can eventually obtain the direction without any lateral slip.

c) Sensing strategy: The main goal is to find the pushing direction that avoids lateral slip. Once we find such a direction, the problem reduces to that of a planar active antenna, discussed in Section II. Fig. 10 shows the sensing strategy to find the direction avoiding any lateral slip.

i) First trial: For the first trial, the antenna is pushed toward an arbitrary direction $\varphi^{(1)}$ [upper script (i) means ith trial]. Let $\psi^{(1)}$ be the direction of contact force obtained by the first pushing motion. When $\delta = \pi$, we can obtain the contact distance immediately from the rotational compliance computed by both the torque increment and the angular displacement. Later on we assume the case of $\delta < \pi$. Extension of the analysis to the case of $\delta > \pi$ is straightforward. From the
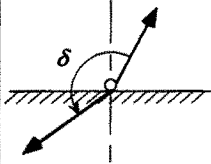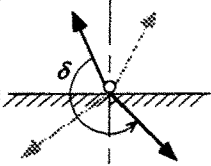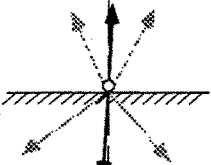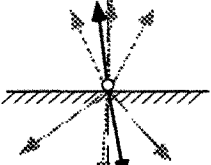
Trial number		Maximum force deviation angle from the normal direction
1st		α
2nd		α
3rd		$\dfrac{\alpha}{2}$
4th		$\dfrac{\alpha}{2}$
i th ($i \geq 4$)		$\dfrac{\alpha}{2^{i-3}}$

Fig. 10. Explanation of the sensing algorithm.

pattern shown in Fig. 9, the sensor system can recognize a slip in the left direction. It should be noted that the following discussion holds irrespective of initial δ.

ii) Second trial: The second pushing direction is chosen so that the slip may appear in the opposite direction against the first one. This can be achieved by choosing the pushing direction in the following way:

$$\varphi^{(2)} = \varphi^{(1)} - \text{sign}[\delta^{(1)} - \pi] \cdot \frac{\pi}{2} \qquad (15)$$

where $\delta^{(1)} = \varphi^{(1)} - \psi^{(1)}$. When choosing the second pushing direction according to (15), $\psi^{(1)}$ and $\psi^{(2)}$ always lie in two different regions, namely, one is in the right half plane with respect to the outer normal vector, and the other is in the left one. Since the contact force projected on Π can always exist within the boundary of the dynamic friction cone projected on Π, the following condition holds:

$$\nu^+ = -\frac{\alpha}{2} < \frac{\psi^{(1)} + \psi^{(2)}}{2} < \nu^+ + \frac{\alpha}{2}. \qquad (16)$$

Equation (16) implies that the angle between ν^+ and the arithmetic mean of $\psi^{(1)}$ and $\psi^{(2)}$ is less than $\alpha/2$.

iii) Third trial: The third pushing direction is chosen so that the extended line may divide $\psi^{(1)}$ and $\psi^{(2)}$ equally, namely

$$\varphi^{(3)} = [\psi^{(1)} + \psi^{(2)}]/2 + \pi. \qquad (17)$$

From (16) and (17), the difference between $\psi^{(3)}$ and ν^+ is at most $\alpha/2$. This means that after the third trial, the contact force projected on Π exists within the cone whose angle is less than the half of the dynamic friction cone. This nature can be conveniently exploited in estimating the sensing accuracy.

iv) ith trial (i $\geq$ 4): Picking up $\psi^{(i-1)}$ and $\psi^{(k)}$ ($1 \leq k \leq i-2$), we choose the ith pushing direction in the following way:
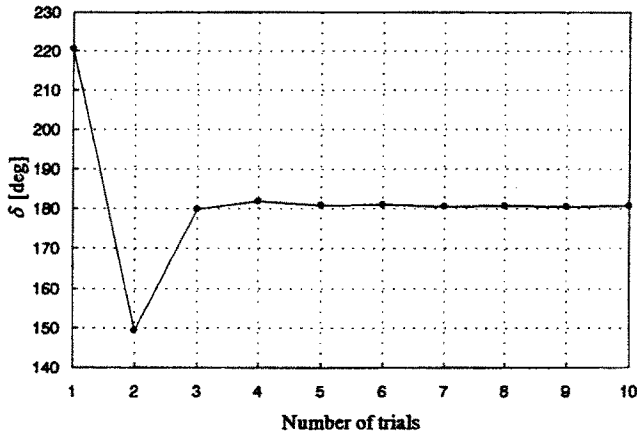
$$\varphi^{(i)} = [\psi^{(i-1)} + \psi^{(k)}]/2 + \pi \qquad (18)$$

where $\{k | [\psi^{(i-1)} - \nu^+][\psi^{(k)} - \nu^+] < 0 \cap \min |\psi^{(k)} - \nu^+|, 1 \leq k \leq i-2\}$. Note that by examining δ we can evaluate the sign of $\psi^{(j)} - \nu^+ (1 \leq j \leq i-1)$ and how close the pushing direction is to ν^+, although the direction of ν^+ is unknown. Equation (18) means that the pushing direction is determined so that the normal direction ν^+ always exists between $\psi^{(i-1)}$ and $\psi^{(k)}$. By choosing the pushing direction in this way, the maximum angle deviation between the contact force projected on Π and the outer normal direction is given by
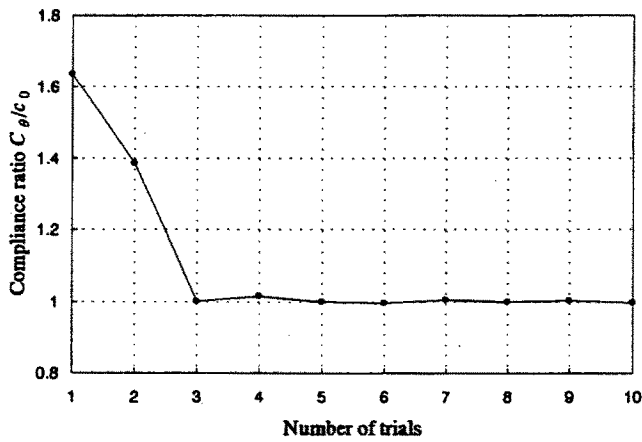
$$\max |\psi^{(i)} - \nu^+| < \frac{\alpha}{2^{i-3}}, \qquad i \geq 4. \qquad (19)$$

Since $\lim_{i \to \infty} \alpha/2^{i-3} = 0$, $\lim_{i \to \infty} \psi^{(i)} = \nu^+$, the direction of contact force finally converges to the outer normal direction on Π. Namely, the pushing direction coincides with the inner normal direction on Π. Thus, we can find the normal direction projected on Π. Once we detect such direction, the contact distance can be obtained by simply computing the rotational compliance, because the rotational compliance under no lateral slip becomes a function of the contact distance alone. Thus, the convergence of the algorithm is ensured if an infinite number of active motions are allowed, while it is not an efficient way.

Fig. 11(a) and (b) show typical experimental results, where the convergence process of δ and C_θ/c_0 are plotted with respect to the number of trial, respectively. It should be noted that both δ and C_θ/c_0 converges very quickly as the number of trial increases. With three times trials, both δ and C_θ/c_0 almost reach their equilibrium points. When $C_\theta \approx c_0$, we can obtain the contact distance accurately, since c_0 represents the rotational compliance obtained under the pushing motion toward ν^-. Fig. 12 also shows an experimental result, where the relationship between ith pushing direction and the direction of ith contact force is expressed by arrows. For the first pushing, the antenna makes a lateral slip toward the left side. For the second one, it again results in failure in avoiding a lateral slip and as a result it moves toward the right side. The third pushing direction computed by (18) provides nearly the inner normal direction, and, therefore, the direction of contact force is very close to the outer normal direction.

(a)

(b)

Fig. 11.   Convergence process for δ and C_θ/c_0: (a) δ versus the number of trials and (b) C_θ/c_0 versus the number of trials.
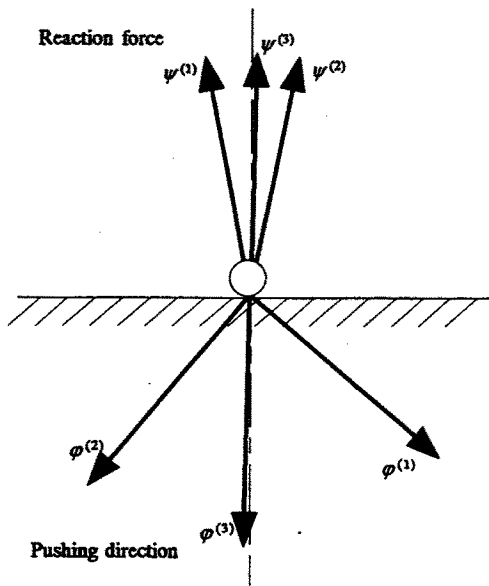

Fig. 12.   The relationship between $\varphi^{(i)}$ and $\psi^{(i)}$.

d) When can we stop the trials?: A natural question that comes up is when we can stop the trials. In other words, how many active motions are really necessary for keeping
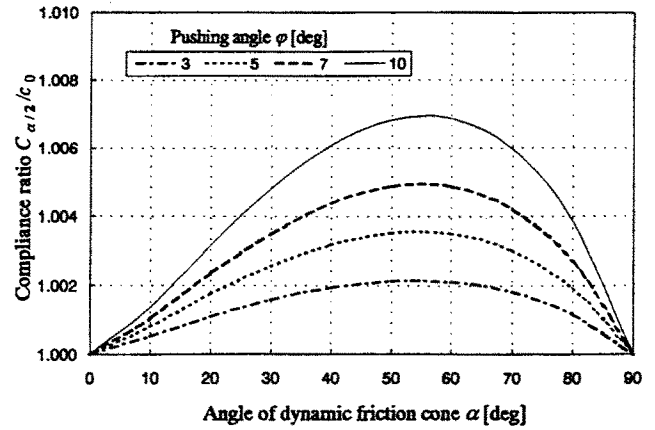

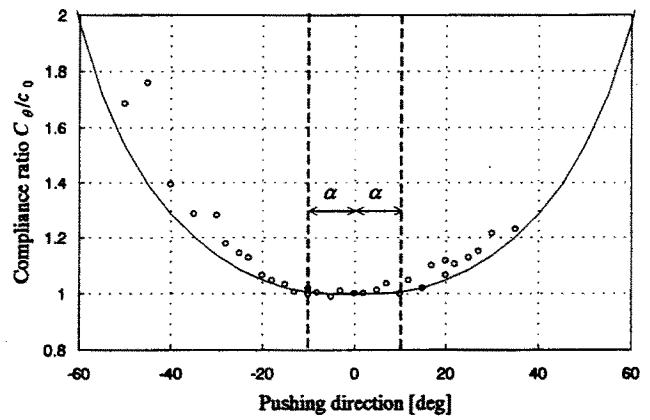Fig. 13.   Compliance ratio when pushing to $\alpha/2$ from normal direction.

Fig. 14.   The relationship between C_θ/c_0 and φ ($\alpha = \pi/18$, $\Delta\theta = \pi/36$).

a sufficient accuracy? Fig. 13 shows the compliance ratio $C_{\alpha/2}/c_0$ when the pushing motion is imparted in the direction of $\alpha/2$ from ν^-, where $C_{\alpha/2}$ denotes the compliances under the pushing motion in the direction of $\alpha/2$ from ν^-. From this figure, it can be found that if the pushing direction is selected within $\alpha/2$ from ν^-, it is ensured that the theoretical sensing error can be kept within the range of 1% irrespective of the size of the dynamic friction cone. By combining the results in Figs. 11 and 13, we can say that three active motions are sufficient for keeping less than 1% of theoretical sensing error.

Finally, Fig. 14 shows the relationship between the pushing direction φ and compliance ratio, where the real line denotes the analytical result and the circles show the experimental results. Experimental results demonstrate a remarkable closures of C_θ and c_0 when the pushing angle lies in the range $[-\alpha/2,\ \alpha/2]$, which supports our analytical result. The precise derivation of $C_{\alpha/2}$ is given in the Appendix.

e) Example of contour sensing: Fig. 15 shows an example of contour sensing, where the experiment is executed for a box. The circles represent the points detected by applying the proposed contact point-sensing strategy. It needs at least three trials for detecting the first contact point with the theoretical sensing error of less than 1%. For finding the next contact point, the first pushing motion is given in the same direction as that obtained in the last trial for detecting the former contact point. This approach is based on the idea that the normal
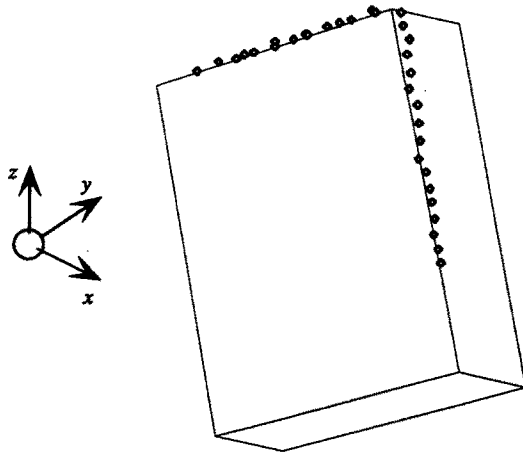
Fig. 15. Experimental result of the contour sensing.

Fig. 16. Analytical model and definition of parameters.

direction at ith contact point is usually not so different from that at $(i - 1)$th contact point. This approach provides us with a time efficient sensing. For the prototype model, the sensing speed for one trial is 1.5 s, which leads 4.5 s for localizing one contact point.

IV. EFFECT OF THE ENVIRONMENT'S CURVATURE ON THE SENSING ACCURACY

So far, with Assumptions A-9 and B-2, we assumed that the antenna makes contact with a sharp edged object, and therefore, the contact point on the environment does not change or the shift is negligibly small, while the contact point along the antenna continuously moves during a pushing motion to satisfy the geometrical relationship between the antenna shapes before and after the bending deformation. When the environment has a finite curvature, the contact point moves continuously on the environment during the pushing motion. As a result, the contact point will shift toward the joint of the antenna. Since a calibration test as shown in Fig. 6 is normally done for a sharp edged object, it is important to evaluate in advance how a large sensing error is expected by the environment's geometry.

Since the antenna motion is finally reduced into a planar motion even in the case of the 3-D active antenna, without losing generality, we can consider 2-D active antenna contacting an environment as shown in Fig. 16. Here s_x and s are the initial contact length and the final contact length, respectively, and the dotted line denotes the tangent to the antenna's shape at the base point. The lower subscripts "i" and "f" denote initial and final values, respectively. If the environment has a sharp edge at the initial contact point, s_x and s should be exactly same. However, they are no longer same when it has an appropriate curvature at the point of contact with the antenna. We assume that the object shape is described implicatively by the following equation: $G(r) = 0$, where r is a position vector whose origin is given at an arbitrary point as shown in Fig. 16. Here in this figure, and ξ_1 and ξ_2 are the unit vectors perpendicular each other. For our convenience, we choose the direction of ξ_1 is so determined that it coincides with the longitudinal direction of the initial beam posture.
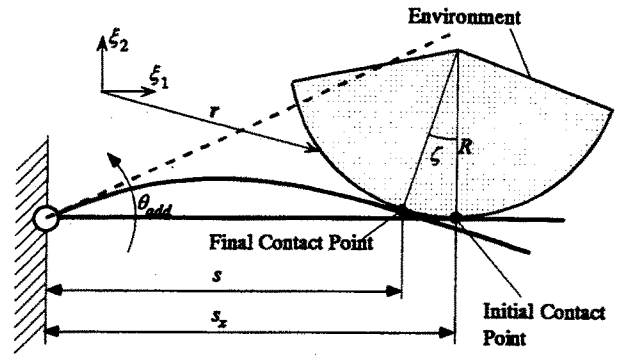
First of all, let us qualitatively consider the effect of the shift of the contact point during sensing. As seen from Fig. 16, the shift of the contact point can be decomposed into the $-\xi_1$ and ξ_2 directional shifts, which bring two different effects for the rotational compliance around the base. The $-\xi_1$ directional shift contributes to reducing the rotational compliance, while the ξ_2 directional one contributes to increasing it. Thus, these two shifts act on the rotational compliance so that they may cancel each other, though the degree of cancellation strongly depends on the environment's curvature at the point of contact, on the contact length, and on how a large pushing angle is imparted. Let us now focus on the intersection between the initial and the final beam postures. For a sharp edged environment, this intersection coincides with the initial contact point. For an appropriate curved environment, this intersection always shifts toward the base of the beam. This means that under a constant pushing angle θ_{add}, the torque increase for a curved environment is always larger than that for an edged environment, which proves $C_{\theta c} < C_{\theta e}$ where the subscript "c" and "e" denotes curved and an edged environments, respectively. Therefore, the sensor system always provides a shorter distance for a curved environment than that for an edged one.

Since the ξ_1 directional shift of the contact point is expressed by the scalar product $-\xi_1^t(r_f - r_i)$, $s_x - s$ is given by

$$s_x - s = -\xi_1^t(r_f - r_i). \tag{20}$$

Similarly, since the ξ_2 directional shift of the contact point is expressed by $\xi_2^t(r_f - r_i)$, the geometrical balance in the ξ_2 direction is given by

$$\frac{fs^3}{3EI} = s\theta_{add} - \xi_2^t(r_f - r_i). \tag{21}$$

Since a normal direction on the environment's surface is represented by $\nabla G(r)$, ζ defined in Fig. 18 is given by

$$\zeta \approx \tan \zeta = \frac{\|\nabla G(r_f) \times \nabla G(r_i)\|}{\nabla G(r_f) \cdot \nabla G(r_i)}. \tag{22}$$

Since the displacement angle of the antenna is equal to $\zeta + \theta_{add}$, there holds

$$\frac{fs^2}{2EI} + \theta_{add} + \zeta. \tag{23}$$

The joint torque and the rotational compliance $C_{\theta c}$ expressed by $\tau = sf$ and $C_{\theta c} = \theta_{add}/\tau$. Equations (21)–(23) form a set of basic equations for solving the relationship between the contact distance s and the rotational compliance $C_{\theta c}$. Since the local environment's shape has a constant radius R, we can use a circular object instead of an environment without the loss of generality. Thus, hereafter, we study a circular object with the following mathematical form:

$$G(r) = \|r - r_0\| - R = 0 \tag{24}$$

where r_0 is the position vector pointing the center of the circle. From (24)

$$\nabla G(r) = \frac{r - r_0}{R}. \tag{25}$$

Therefore, we obtain

$$\|\nabla G(r)\| = \frac{\|r - r_0\|}{R} = 1. \tag{26}$$

By taking (25) into consideration, $r_f - r_i$ is alternatively expressed by

$$r_f - r_i = R\{\nabla G(r_f) - \nabla G(r_i)\}. \tag{27}$$

Since

$$\xi_2 = -\frac{\nabla G(r_i)}{\|\nabla G(r_i)\|} = -\nabla G(r_i) \tag{28}$$

the ξ_2 directional shift of the contact point is given by the scalar product

$$\begin{aligned}
\xi_2^t(r_f - r_i) &= -\{\nabla G(r_i)\}^t R\{\nabla G(r_f) - \nabla G(r_i)\} \\
&= -R\|\nabla G(r_f)\|\|\nabla G(r_i)\|\cos\zeta + R\|\nabla G(r_i)\|^2 \\
&= R(1 - \cos\zeta). \tag{29}
\end{aligned}$$

On the other hand, taking into account the relationship $\xi_2 = -\nabla G(r_i)$

$$\begin{aligned}
-\xi_1^t(r_f - r_i) &= -\xi_1^t R\{\nabla G(r_f) - \nabla G(r_i)\} \\
&= -\xi_1^t R\{\nabla G(r_f) + \xi_2\} \\
&= -R\|\nabla G(r_f)\|\|\xi_1\|\cos\left(\zeta + \frac{\pi}{2}\right) \\
&= R\sin\zeta. \tag{30}
\end{aligned}$$

By replacing $\xi_1^t(r_f - r_i)$ and $-\xi_2^t(r_f - r_i)$ with $R(1 - \cos\zeta)$ and $R\sin\zeta$, respectively, we finally obtain

$$s_x - s = R\sin\zeta, \tag{31}$$

$$\frac{fs^3}{3EI} = s\theta_{add} - R(1 - \cos\zeta). \tag{32}$$

Taking the linear approximation of the trigonometric functions, we can derive the following equation:

$$3EIC_{\theta c} = k(h)s_x \tag{33}$$

where

$$k(h) = 1 - \frac{1}{2h} \tag{34}$$

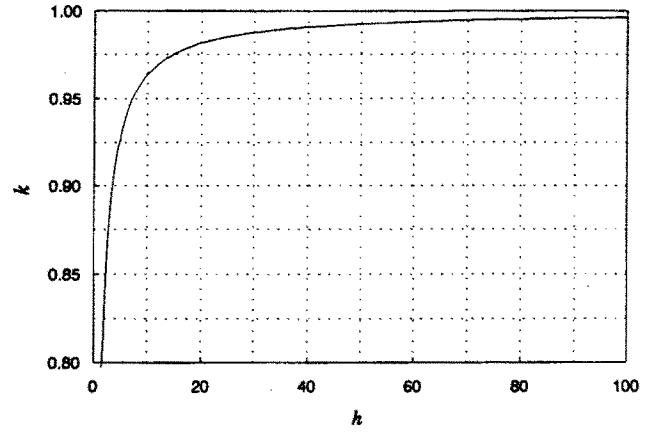$$h = \frac{s_x}{R\theta_{add}}. \tag{35}$$

Fig. 17. The relationship between k and h.

Defining the rotational compliance for an edged environment with $C_{\theta e}$, we have the following relationship for such an environment [1]

$$3EIC_{\theta e} = s_x. \tag{36}$$

By dividing each side of (33) by (36), we can obtain

$$\frac{C_{\theta c}}{C_{\theta e}} = k(h). \tag{37}$$

Therefore, $k(h)$ denotes the ratio of the rotational compliance for a circular and an edged environments. For example, $k(h) = 0.99$ means that the theoretical sensing error between a circular and an edged environments is 1%. $k(h)$ is a function of h alone. Since h is composed of the contact distance, the radius of the curvature of the environment, and the pushing angle, the sensing error is also affected by these physical parameters. But an important feature is that the influence on the sensing error is the same if the nondimensional parameter h is identical. Fig. 17 shows the map of $k(h)$ for various h. As h increases, k sharply increases and asymptomatically approaches to unity for an infinite h. Since an edged environment with a negligibly small R at the point of contact is equivalent to an infinite h, the convergence to unity for an infinite h in Fig. 17 is quite reasonable and matches with our intuition. The nondimensional parameter h given by (35) further suggests that either a contact with extremely long distance from the base or a negligibly small pushing angle also produces a similar effect on the sensing accuracy. Among s_x, R, and θ_{add}, when the antenna makes contact, both s_x and R are automatically determined and not controllable. The controllable parameter in h is θ_{add} only. So, we must keep θ_{add} small so that we can make the sensing error small.

Usually antenna should be in a long and slender shape and, therefore, the compliance of the beam is very high. It means that the sensor has to have very sensitive torque sensor to measure the very small torque produced by the minute rotation. Therefore, choosing a too small θ_{add} is not desirable from the viewpoint of obtaining a large reaction torque. When the base part of antenna makes contact with an object, the torque sensor can receive a sufficiently large reaction torque, even under a small θ_{add}. The most problematic situation occurs when the tip
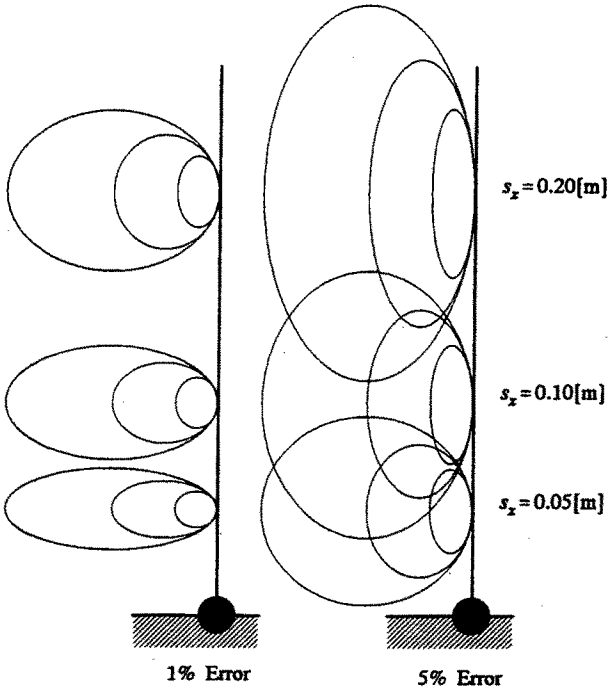
Fig. 18. Objects' shape whose sensing errors result in 1 and 5%, where closed curve represent a solid object.

Fig. 19. Experimental results for k.

part of the antenna makes contact with the object. Because the reaction torque becomes extremely small under the same θ_{add}. Now, recall the nondimensional parameter $h = s_x/(R\theta_{add})$ and an important feature that the influence on the sensing error is same if h is identical. This nature suggests a reasonable procedure for determining the final pushing angle.

1) We choose a reference θ_{add} that ensures a tolerable error if the antenna makes contact with an object under $s_x = s_{xd}$ and $R \leq R_d$, where s_{xd} and R_d are the reference contact distance and the reference radius of curvature, respectively, and θ_{add} should be chosen so that the torque sensor will receive a sufficiently detectable reaction torque under $s_x = s_{xd}$. Then, a sensing motion is started.

2) When the computed distance s_x is not equal to s_{xd}, $\theta_{add new}$ is determined such that $s_{xd}/\theta_{add} = s_x/\theta_{add new}$, where this relationship corresponds to keeping the sensing accuracy constant under the same radius of curvature.

Note that $\theta_{add new}$ increases when s_x is larger than s_{xd}, which contributes to increasing the reaction torque. Since the contact distance can be computed at every sampling time, the suggested procedure can be executed in real time and, therefore, multiple pushing motions are not necessary in practical application. Thus, there are two advantages for this procedure, one is that the pushing angle θ_{add} is adaptively chosen so that the sensing accuracy can be identical irrespective of the contact distance, and the other is that it greatly contributes to increasing the reaction torque when the tip part of the antenna makes contact with the object. However, apart from this procedure, we would note that if we utilize a beam based on the design orientation given in Appendix A, the compliance
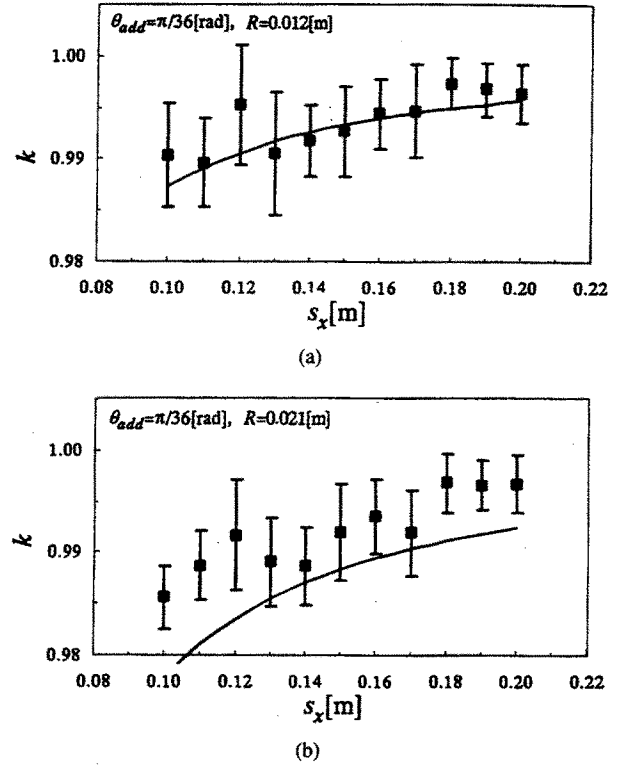
is not as high as that of insect's antenna. As a result, the torque sensor can measure the reaction force even under a minute rotation of the antenna base.

Fig. 18 visually illustrates objects' shape whose sensing error lead to 1 and 5%, where the pushing angle is fixed to $\theta_{add} = \pi/36$ rad. Since the calibration test is done for an edged environment, it is desirable that the rotational compliance is insensitive to the curvature of the environment at the point of contact. It can be seen from Fig. 18 that the influence of the environment's curvature on the sensing error is is suppressed, unless the radius of curvature is extremely large and the contact happens just close to the base.

Fig. 19 shows experimental results for two curved objects [(a) $R = 0.012$ m and (b) $R = 0.002$ m], where the squares denote the mean values for fifteen trials and the upper and the lower bounds denote the standard deviation. The real lines in Fig. 19 correspond to the theoretical ones in Fig. 17, where h is represented by the contact distance s_x. Since the vertical axis is partially enlarged, it should be noted that the standard deviations appearing in Fig. 19 are not as large as those coming from our visual image. It can be seen from Fig. 19 that the experimental results exhibit less than unity but very close to unity, which supports the analytical result. Also, the qualitative tendency of the experimental results coincide with the theoretical lines, while there are a bit quantitative difference between them.

V. DISCUSSION

In this section, we consider to partly relax the assumptions given in groups A and B. Assumption A-1 claims that the object is rigid, which might be a strong restriction. First of
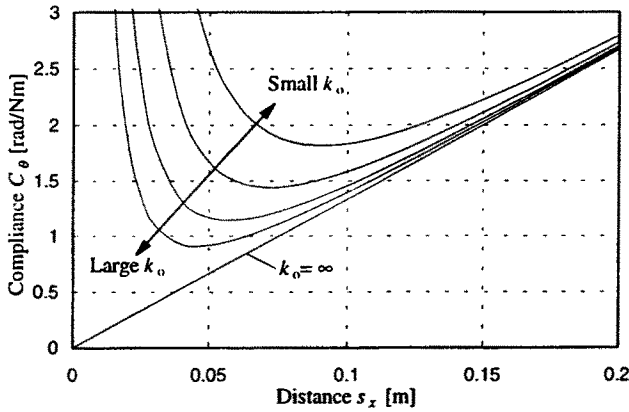
Fig. 20. The relationship between sensed compliance C_θ and contact distance s_x.

all, we discuss how to cope with a compliant object. Since the proposed method can detect the contact distance through the rotational compliance of the antenna in contact with an object, it can not be used as it is when the object is not rigid. Now, suppose that the sensor system is implemented into a mobile robot or the base can be moved by additional actuators. In such a case, the antenna can touch the same object with two different contact points. Let k_o be the stiffness of the object. The sensed compliance at the rotational center is given by,

$$C_{\theta 1} = \frac{s_x}{3EI} + \frac{1}{s_x^2 k_o}, \tag{38}$$

where $C_{\theta 1}$ denotes the sensed compliance when the antenna makes contact with the object at the contact length s_x. Equation (38) means that the sensed compliance is composed of those from the antenna and the object, respectively. Fig. 20 shows the relationship between the sensed compliance C_θ and the contact distance s_x, where the parameter is the stiffness of object. Now, let us assume that after obtaining $C_{\theta 1}$ at $s_x = s_x$, the mobile robot is moved by Δs and, once again, $C_{\theta 2}$ is measured, where $C_{\theta 2}$ denotes the sensed compliance when the antenna makes contact with the object at the contact length $s_x - \Delta s$. Substituting $s_x - \Delta s$ into (38) yields

$$C_{\theta 2} = \frac{s_x - \Delta s}{3EI} + \frac{1}{(s_x - \Delta s)^2 k_o}. \tag{39}$$

From (38) and (39), we can finally obtain

$$3(EIC_{\theta 1} - EIC_{\theta 2} - \Delta s)s_x^2 + 3\Delta s(2EIC_{\theta 2} + \Delta s)s_x$$
$$- 3EIC_{\theta 2}\Delta s^2 - \Delta s^3 = 0. \tag{40}$$

Since (40) can be regarded as the second order equation with respect to s_x, we can easily solve it as follows:

$$s_{x1} = \frac{\Delta s(6EIC_{\theta 2} + 3\Delta s - \sqrt{D})}{6EI(C_{\theta 2} - C_{\theta 1}) + 6\Delta s} \tag{41}$$

$$s_{x2} = \frac{\Delta s(6EIC_{\theta 2} + 3\Delta s + \sqrt{D})}{6EI(C_{\theta 2} - C_{\theta 1}) + 6\Delta s}. \tag{42}$$

Here $D \equiv 36(EI)^2 C_{\theta 1} C_{\theta 2} + 12EI(C_{\theta 1} - C_{\theta 2})\Delta s - 3\Delta s^2$.

While there are two solutions s_{x1} and s_{x2}, we can easily prove that $0 < s_{x1} < \Delta s < s_{x2}$. Since $s_x - \Delta s$ should be positive, the solution s_{x1} is not appropriate. Thus, we have

always one solution s_{x2} matching with the condition $s_x - \Delta s > 0$. Once s_x is determined, the stiffness k_o is automatically computed by using (38).

Now, let us consider the contact mode when the tip of the antenna touches an object which will most probably occur in ordinary sensing motion. Note that the rotational compliance coming from the object decreases according to $1/s_x^2$ as shown in (38), while the compliance from the antenna increases in proportion to s_x. This means that the rotational compliance from the object gives the smallest effect on the measured compliance when the tip of the antenna touches the object, while the compliance from the antenna provides the largest one. Such a behavior of the object's stiffness can be also observed in Fig. 20. If the object is rigid enough, the antenna can easily recognize from the measured compliance whether the tip of the antenna touches the object or not. Because the measured compliance exhibits the largest value under such a situation. Of course, in case that the object has similar compliance compared with the equivalent compliance at the tip of the antenna, the antenna cannot classify whether the tip makes contact with a rigid object or an inner point makes contact with a compliant object.

VI. CONCLUSION

In this paper we proposed a new active sensing system, called active antenna, and demonstrated that under no lateral slip, the contact distance is simply proportional to the rotational compliance alone, if the environment's curvature is small and the environment's stiffness is large. We considered how to detect the lateral slip from available sensors, and showed that this can be done by using the two-axis moment sensor. We further showed that even under the lateral slip during the first active motion, the proposed algorithm can eventually reach the pushing direction without any lateral slip, and the contact distance can be obtained with the normal direction on the sensing plane II. We also showed that three active motions were needed for detecting the contact distance with the theoretical sensing error of less than 1%. We also discussed the effect of environment's curvature on the sensing error and showed that its influence is kept within a few percentages, unless the radius of curvature is large or the contact occurs close to the base.

APPENDIX A
DESIGN ORIENTATION OF ANTENNA GEOMETRY

A slender antenna is not always in straight-line shape and it will easily deform for an external force, such as gravitational force. By applying classical beam theory, we can evaluate the deformation of the antenna. As for the design of the sensing system, we can determine the antenna length based on the maximum deflection $w_{\max}$ at the tip of the antenna under the gravitational force. For the antenna placed horizontally, we expect the maximum deflection. Under such a situation, $w_{\max}$ is given by

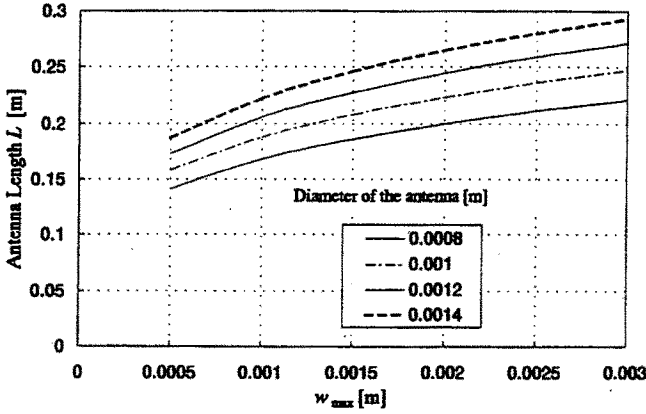$$w_{\max} = \frac{8\rho g L^4}{E d^4} \tag{43}$$

Fig. 21. The relationship between the antenna length L and the maximum deflection w_{max}.

Fig. 22. The relationship between δ and φ ($\alpha = \pi/18$, $\Delta\theta = \pi/36$).

where g and ρ are the gravitational acceleration and the density per unit length of the antenna, respectively. Fig. 21 shows the relationship between the antenna length L and w_{max}. Assume the beam having the diameter of 0.8 mm. Fig. 21 tells us that the antenna length L having less than 210 mm allows us to suppress w_{max}/L within 1%. Based on this consideration, we finally determined the antenna length L and diameter d as follows:

$$L = 210\,\text{mm}$$
$$d = 0.8\,\text{mm}.$$

Therefore, the deformation from straight-line shape is at most 1% under the gravitational field. Although this is not always the case under a strong acceleration field, we believe that this design provides a reasonable orientation. Because the antenna's motion during contact is planned slow enough to ensure that a large inertia force is suppressed.

APPENDIX B
ESTIMATION OF THE LATERAL SLIP BASED SENSING ERROR

Let us discuss the relationship between the pushing direction and the direction of the contact force. For a compound pushing angle $\Delta\theta$, the lateral slip s_{lat} can be given by

$$s_{lat} = s_x \Delta\theta(\cos\lambda - \sin\lambda\tan\beta) \quad (44)$$

where λ is the angle between object's surface and pushing direction and given by $\lambda = \varphi - \nu^+ - \pi/2$. From the geometrical relationship, the effective displacement vector $\Delta r_e^{s+\Delta}$ is given by

$$\|\Delta r_e^{s+\Delta}\| = s_x \Delta\theta\, \frac{\sin\lambda}{\cos\beta}. \quad (45)$$

The contact point in the antenna makes a slip in the direction expressed by the ratio of the changing rate of the lateral slip $\dot{s}_{lat}$ and that of the longitudinal slip $\dot{s}_{lon}$, which eventually provides the following relationship [25]:

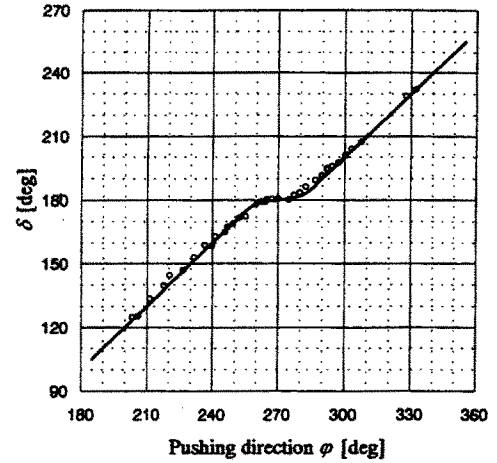$$\tan\gamma = \frac{d}{d\Delta\theta}(s_{lat}) \bigg/ \frac{d}{d\Delta\theta}(s_{lon}). \quad (46)$$

Here, we assume that the changing rate of s_{lon} with respect to $\Delta\theta$ is given by the following equation:

$$\frac{d}{d\Delta\theta}(s_{lat}) = ks_x\Delta\theta\,\frac{\sin\lambda}{\cos\beta} \quad (47)$$

where k is a positive constant and determined by solving the load-deformation equation of the beam. Actually, the model given by (47) provides a very good approximation with experimental data. Finally, considering the geometrical relationship of $\tan\beta = \tan\alpha\sin\gamma$, we obtain

$$\tan\beta - \tan\alpha\sin\left[\tan^{-1}\left(\frac{\cos\lambda - \sin\lambda\tan\beta}{k\Delta\theta\sin\lambda/\cos\beta}\right)\right] = 0. \quad (48)$$

Considering further geometrical relationships, $\lambda = \varphi - \nu^+ - \pi/2$ and $\beta = \nu^+ - \psi$, we can obtain the following form from (48):

$$\psi = g_1(\varphi, \Delta\theta, \nu^+, \alpha). \quad (49)$$

As an example of the function $g_1(\varphi, \Delta\theta, \nu^+, \alpha)$, let us assume the pushing motion for the environment whose outer normal direction ν^+ is equal to $\pi/2$ and the friction angle α to $\pi/18$. We also assume the pushing angle of $\Delta\theta = \pi/36$. Fig. 22 shows the relationship between the pushing direction φ and δ, where the real line denotes the analytical result and the circles show the experimental results. The matching between analytical and experimental results is fairly good, which suggests the validation of the analysis taken here. The important feature is that φ is the simply increasing function with respect to δ. Also we would remark that δ is very close to π, when the pushing direction is so selected that it can enter the dynamic friction cone. Because of this particular feature, the compliance obtained for a pushing motion whose direction exists within the friction cone is not so different from that obtained for the normal direction.

REFERENCES

[1] R. A. Russell, "Closing the sensor-computer-robot control loop," *Robot Age*, pp. 15–20, Apr. 1984.

[2] S. S. M. Wang and P. M. Will, "Sensors for computer controlled mechanical assembly," *Ind. Robot*, pp. 9–18, Mar. 1978.

[3] R. A. Russell, "Object recognition using articulated whisker probes," in *Proc. 15th Int. Symp. Industr. Robots*, 1985, pp. 605–612.

[4] P. McKerrow, *Introduction to Robotics*. Reading, MA: Addison-Wesley, 1990.

[5] R. A. Brooks, "A robot that walks; Emergent behaviors from a carefully evolved network," *Neural Computat.*, vol. 1, pp. 253–262, 1989.

[6] S. Hirose et al., "Titan III, A quadruped walking vehicle," in *Proc. 2nd Int. Symp. Robot Res.*, Cambridge, MA, 1985.

[7] E. N. Schiebel, H. R. Busby, and K. J. Waldron, "Design of a mechanical proximity sensor," *Robotica*, vol. 4, pp. 221–227, 1986.

[8] R. A. Russell, "Using tactile whiskers to measure surface contours," in *Proc. 1992 IEEE Int. Conf. Robot. Automat.*, 1992, pp. 1295–1300.

[9] J. F. Wilson and U. Mahajan, "The mechanics and positioning of highly flexible manipulator limbs," *ASME J. Mech., Transm., Automat. Des.*, vol. 111, pp. 230–237, 1989.

[10] J. M. Snyder and J. F. Wilson, "Dynamic of the elastica with end mass and follower loading," *ASME J. Appl. Mech.*, vol. 57, pp. 203–208, 1990.

[11] J. F. Wilson and A. Chen, "A whisker probe system for shape perception of solids," *ASME J. Dyn. Syst., Meas., Contr.*, vol. 117, pp. 104–108, 1995.

[12] T. Tsujimura and T. Yabuta, "A tactile sensing method employing force/torque information through insensitive probes," in *Proc. 1992 IEEE Int. Conf. Robot. Automat.*, 1992, pp. 1315–1320.

[13] J. K. Salisbury, "Interpretation of contact geometries from force measurements," in *Proc. 1st Int. Symp. Robot Res.*, 1983.

[14] D. L. Brock and S. Chiu, "Environment perception of an articulated robot hand using contact sensors," in *Proc. IEEE Int. Conf. Robot Automat.*, Raleigh, NC, 1987, pp. 89–96.

[15] T. Tsujimura and T. Yabuta, "Object detection by tactile sensing method employing force/moment information," *IEEE Trans. Robot. Automat.*, vol. 5, 1988.

[16] A. Bicchi, "Intrinsic contact sensing for soft fingers," in *Proc. IEEE Int. Conf. Robot. Automat.*, Cincinnati, OH, 1990, p. 968.

[17] M. Kaneko and K. Tanie, "Contact point detection for grasping of an unknown object using self-posture changeability," in *Proc. IEEE Int. Conf. Robot. Automat.*, 1990, p. 1057.

[18] _____, "Contact point detection for grasping an unknown object using self-posture changeability," *IEEE Trans. Robot. Automat.*, vol. 10, pp. 355–367, 1994.

[19] M. Kaneko, H. Maekawa, and K. Tanie, "Active tactile sensing by robotic fingers based on minimum-external-sensor-realization," in *Proc. IEEE Int. Conf. Robot. Automat.*, 1992, pp. 1289–1294.

[20] H. Maekawa, K. Tanie, and M. Kaneko, "Active touch using fingertip tactile sensor," in *Proc. IEEE Int. Conf. Intell. Robot. Syst.*, 1992, pp. 1744–1750.

[21] M. Kaneko, "Active Antenna," in *Proc. 1994 IEEE Int. Conf. Robot. Automat.*, 1994, pp. 2665–2671.

[22] M. Kaneko, N. Ueno, and T. Tsuji, "Active Antenna (basic working principle)," in *Proc. 1994 IEEE Int. Conf. Intell. Robot. Syst.*, 1994, pp. 1744–1750.

[23] M. Ishikawa, "An active sensor system using parallel processing circuits," *Trans. SICE*, vol. 24, no. 8, p. 88, 1988 (in Japanese).

[24] S. Timoshenko and D. H. Young, *Elements of Strength of Materials*. New York: Van Nostrand, 1968.

[25] S. Goyal, A. Ruina, and J. Papadopoulos, "Limit surface and moment function descriptions of planar sliding," in *Proc. 1989 IEEE Int. Conf. Robot. Automat.*, 1989, pp. 794–799.

Makoto Kaneko (A'84–M'87) received the B.S. degree in mechanical engineering from Kyushu Institute of Technology, Kyushu, Japan, in 1976, and the M.S. and Ph.D. degrees in mechanical engineering from Tokyo University, Tokyo, Japan, in 1978 and 1981, respectively.

From 1981 to 1990, he was a Researcher at the Mechanical Engineering Laboratory (MEL), Ministry of International Trade and Industry (MITI), Tsukuba Science City. From 1988 to 1989, he was a Post-Doctoral Fellow at Technical University of Darmstadt, Germany, where he joined a space robotics project. From 1990 to 1993, he was an Associate Professor with Computer Science and System Engineering, Kyushu Institute of Technology. From November 1991 to January 1992, he received an Invited Professorship at Technical University of Darmstadt, Germany. Since October 1993, he has been a Professor at the Industrial Engineering Department, Hiroshima University, Hiroshima, Japan. His research interests include tactile-based active sensing, grasping strategy, sensor applications, and experimental robotics.

Dr. Kaneko received the outstanding young engineer award in 1983 from the Japan Society of Mechanical Engineers, the best paper awards from the Robotics Society of Japan in 1994, and from the Japanese Society of Instrumentation and Control Engineers in 1996. He also received the Humboldt Research Award in 1997. He served as an Associate Editor of IEEE TRANSACTIONS ON ROBOTICS AND AUTOMATION from 1990 through 1994. He has been a Program Committee Member for IEEE International Conference on Intelligent Robots and Systems since 1991. He also worked as a Program Committee member for the 1995, 1996, and 1998 IEEE International Conference on Robotics and Automation. He is a member of the IEEE Robotics and Automation Society, the IEEE Systems, Man, and Cybernetics Society, and the IEEE Industrial Electronics Society. He is also a member of Japan Society of Mechanical Engineers, Robotics Society of Japan, and Japanese Society of Instrumentation and Control Engineers.

Naoki Kanayama received the B.S. degree in mechanical system engineering from Kyushu Institute of Technology, Fukuoka, Japan, in 1994, the M.S. degree in information engineering from Hiroshima University, Hiroshima, Japan, in 1996, and is currently pursuing the Ph.D. degree.

His current research interest is active sensing.

Mr. Kanayama received the outstanding young engineer award, Robotics Society of Japan, in 1994. He is a Research Fellow of the Japan Society for the Promotion of Science.

Toshio Tsuji (A'88) was born in Kyoto, Japan, on December 25, 1959. He received the B.E. degree in industrial engineering, and the M.E. and Doctor of Engineering degrees in system engineering from Hiroshima University, Higashi-Hiroshima, Japan, in 1982, 1985, and 1989, respectively.

From 1985 to 1994, he was a Research Associate in the Faculty of Engineering, Hiroshima University, and was a Visiting Researcher at the University of Genova, Italy, from 1992 to 1993. He is currently an Associate Professor in the Department of Industrial and Systems Engineering, Hiroshima University. He has been interested in various aspects of motor control in robot and human movements.

Dr. Tsuji is a member of the Japan Society of Mechanical Engineers, the Robotics Society of Japan, and the Japanese Society of Instrumentation and Control Engineers.